I&EC research
Industrial & Engineering Chemistry Research

Article

pubs.acs.org/IECR

Run-to-Run-Based Model Predictive Control of Protein Crystal Shape in Batch Crystallization

Joseph Sang-Il Kwon,[†] Michael Nayhouse,[†] Gerassimos Orkoulas,[†] Dong Ni,*[,‡] and Panagiotis D. Christofides*[,†,§]

[†]Department of Chemical and Biomolecular Engineering and [§]Department of Electrical Engineering, University of California, Los Angeles, California 90095, United States

[‡]Institute of Automation, Chinese Academy of Sciences, Beijing 100190, China

ABSTRACT: In this work, we develop a novel run-to-run-based model predictive controller (R2R-based MPC) for a batch crystallization process with process drift and inherent variation in solubility and crystal growth rates. In order to achieve the production of crystals with desired product qualities, a conventional MPC system with nominal process model parameters is initially applied to a batch protein crystallization process. However, the mismatch between the process model and the actual process dynamic behavior because of the process drift and variability becomes severe as batch runs are repeated. To deal with this problem of batch-to-batch variability, after each batch is over, the post-batch crystal attribute measurements, including average crystal shape and size and the number of crystals, are used to estimate off-line the drift of the process model (used in the MPC) parameters from nominal values via a multivariable optimization problem. Along with the adapted controller model parameters, the exponentially weighted moving average (EWMA) scheme is used to deal with the remaining offset in the crystal shape values and thereby to compute a set of optimal jacket temperatures. Furthermore, the crystal growth in the batch crystallization process is modeled through kinetic Monte Carlo simulations, which are then used to demonstrate the capability of the proposed R2R-based MPC scheme in suppressing the inherent variation and process drift in solubility and crystal growth rates. It is demonstrated that the production of crystals with a desired shape distribution is successfully achieved after three batch runs through the use of the proposed R2R-based MPC, while it takes 24 batch runs for the system with the EWMA-type constant supersaturation control to achieve the same objective.

INTRODUCTION

The production of crystals with desired size and shape distributions from batch crystallization processes is a subject of great interest to the pharmaceutical industry. Specifically, crystal size and shape significantly influence the bioavailability of drugs, such as the stability of a carrier to the target site, melting points, and dissolution rates.[1]

In recent years, model predictive control (MPC) of crystallization has received growing attention within the crystallization process community owing to its unique ability to handle constraints on the inputs, the outputs, and the rate of change of inputs.[2−5] Another key benefit of using MPC is its applicability to both dynamic and multi-input/multi-output systems.[6,7] However, the conventional MPC technique is not designed to take advantage of the repetitive nature of batch processes; thus, in most cases the control performance is not improved as batch runs are repeated. Furthermore, the control performance of the MPC is very sensitive to model uncertainties such as changes in the kinetic parameters, which tend to persist from run to run.[8]

Run-to-run (R2R) control uses data from previous batches to adjust controller model/settings for the next batch run.[9−13] Typically, the R2R control methods can be categorized into two distinct classes. For the case of changes in the model parameters, a parameter adaptive control (PAC) scheme, such as the Kalman filter, is applied in order to tune the nominal process model, which is then used to compute control inputs.[14] However, if there is no explicit variation in the model parameters, an offset drift cancellation (ODC) approach, such as exponentially weighted moving average (EWMA), should be employed to estimate the current offset using the post-batch measurements from the past batch runs, and inputs are appropriately computed to compensate for the estimated offset.[15]

While significant efforts have been devoted to the development of the R2R control for semiconductor manufacturing processes,[10,15] very limited attempts have been made to integrate learning-type controls with feedback controls for a variety of chemical processes. For example, the idea of integrating MPC with repetitive control was developed in order to improve the handling of periodic errors and reference trajectories for continuous processes under periodic operation.[16] Another example is an R2R-based concentration control strategy that was proposed for the polymorphic transformation of L-glutamic acid from the metastable α-form to the stable β-form to maximize the yield of β-form.[17] Lastly, an R2R control algorithm integrated with a supersaturation control scheme in cooling crystallization was also investigated.[18]

Special Issue: Scott Fogler Festschrift

Received: June 12, 2014
Revised: July 1, 2014
Accepted: July 3, 2014
Published: July 3, 2014

ACS Publications © 2014 American Chemical Society

dx.doi.org/10.1021/ie502377a | Ind. Eng. Chem. Res. 2015, 54, 4293−4302

Considering the lack of real-time measurements of the product qualities in a standard batch crystallization process, we propose an R2R-based MPC to enhance the controller performance by learning from the past batch runs. Furthermore, the idea of the PAC strategy that estimates controller model parameters and utilizes them for the computation of improved control inputs is borrowed and used along with the ODC scheme. The major benefit of the proposed R2R-based MPC scheme is in its unique capability to deal with the uncertainties and drift in the process while simultaneously satisfying the constraints imposed on the state variables and inputs; this integrated approach will lead to the production of crystals with a desired shape distribution from batch to batch.

More specifically, in the present work, we consider a batch process for the crystallization of lysozyme crystals with uncertainties in the crystal growth rates in the direction of (110) and (101) faces as well as in the solubility. The kinetic Monte Carlo (kMC) simulation developed in the previous work[19] is regarded as a representation of the batch crystallization process and used for the simulation of tetragonal hen egg white (HEW) lysozyme crystals. In order to achieve the production of crystals with a desired shape distribution, the optimal jacket temperature profile is computed from a conventional MPC using a nominal reduced-order moment model and is applied to the first batch. After the first run, the post-batch measurements (e.g., the crystal size and shape distributions and number of crystals) are used to solve a multivariable optimization problem (MOP) off-line for the identification of the process model parameters used in the MPC for the crystal growth rates and solubility. Additionally, the real-time measurements for the solute concentration and temperature in the crystallizer from the previous batch are used in the form of constraints in the MOP to ensure the physical meaning of the process model parameters computed from the MOP. Along with the adapted process model parameters, the EWMA scheme is used to deal with the remaining offset in the crystal shape values and thereby to compute a set of new optimal jacket temperatures. As a result, the production of crystals with a desired shape distribution is achieved by properly suppressing the inherent variation and process drift in the crystal growth rates and solubility. Lastly, the control performance of the proposed R2R-based MPC is compared with those of the conventional MPC and EWMA-type constant supersaturation control (CSC).

MODELING OF BATCH CRYSTALLIZATION PROCESS

In this work, we focus on a batch protein crystallization process (cf. Figure 1), the detailed geometrical parameters of which are taken from ref 20 and presented as follows: a three-blade propeller is used; both the inner diameter and the filling height of the crystallizer are 0.12 m; the clearance height (i.e., the height from the bottom to the impeller) is 0.04 m; and the diameter of the impeller is 0.06 m.

Crystal Nucleation and Growth. The nucleation rate B of lysozyme crystals nucleated at 4% (w/v) NaCl and pH = 4.5 is taken from ref 21 and is presented as follows:

$$B = \begin{cases} 0.041\sigma + 0.063 & \text{for } \sigma \geq 3.11 \\ 8.0 \times 10^{-8} \exp(4.725\sigma) & \text{for } \sigma < 3.11 \end{cases} \quad (1)$$

with units $\mathrm{cm}^{-3}\cdot\mathrm{s}^{-1}$. For simulation and testing of the control performance of the proposed R2R-based MPC control scheme,

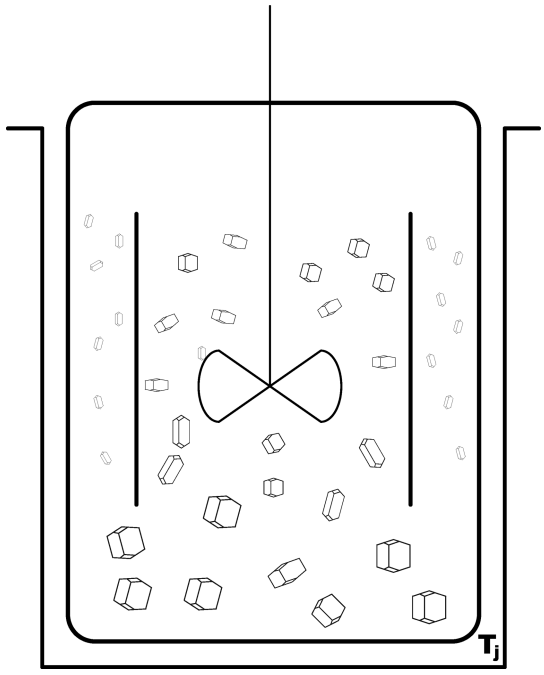

Figure 1. Batch crystallizer configuration.

the degree of secondary nucleation induced by the attrition process among crystals is disregarded. The supersaturation level σ is defined as the logarithmic ratio between the solute concentration C and solubility s (mg/mL) as follows:

$$\sigma = \ln(C/s) \quad (2)$$

where the solubility s is calculated using a second-order polynomial equation, which has been calibrated with the experimental data[22] at 4% (w/v) NaCl and pH = 4.5 and is given as

$$s = 0.0109T^2 - 0.1146T + 1.1773 \quad (3)$$

Note that the temperature T in the crystallizer is in Celsius. The crystal growth is modeled through the kMC simulation using the rate equations presented in Table 1, which were originally developed in ref 23.

Table 1. Surface Processes

reaction	rate equation
adsorption, r_a	$K_0^+ \exp(\sigma)$
desorption, $r_d(i)$	$K_0^+ \exp\left(\frac{\varphi}{k_B T} - i\frac{E_{pb}}{k_B T}\right)$
migration, $r_m(i)$	$K_0^+ \exp\left(\frac{\varphi}{k_B T} - i\frac{E_{pb}}{k_B T} + \frac{E_{pb}}{2k_B T}\right)$

In order to capture the dependencies of the surface processes (e.g., adsorption, desorption, and migration) on the surface micro-configuration, a number of modeling parameters are considered, including the adsorption coefficient K_0^+, the number of nearest neighbors i, the average bonding energy per bond E_{pb}, and the total binding energy ϕ when a molecule is fully surrounded by neighbors (when $i = 4$).[24] In this work, extensive open-loop kMC simulations were executed in order to find a set of physically meaningful E_{pb} and ϕ values for (110) and (101) faces such that the simulated growth rates are calibrated

dx.doi.org/10.1021/ie502377a | Ind. Eng. Chem. Res. 2015, 54, 4293−4302

with the experimental data in the literature. The interested readers may find more detailed information about the development and execution of the kMC simulation for batch processes in ref 19.

Mass and Energy Balance Equations. The mass balance equation that computes the amount of the protein solute C remaining in the continuous phase is given by the following ordinary differential equation (ODE):

$$\frac{dC}{dt} = -\frac{\rho_c}{V_{batch}}\frac{dV_{crystal}}{dt}, \quad C(0) = C_0 \tag{4}$$

where $V_{crystal}$ is the total volume of crystals in the crystallizer, C_0 is the initial protein solute concentration, ρ_c is the crystal density, and V_{batch} is the volume of the batch crystallizer. Similarly, the evolution of the temperature T in the crystallizer is computed from the following ODE:

$$\frac{dT}{dt} = -\frac{\rho_c \Delta H_c}{\rho C_p V_{batch}}\frac{dV_{crystal}}{dt} - \frac{U_c A_c}{\rho C_p V_{batch}}(T - T_j), \quad T(0) = T_0 \tag{5}$$

where T_j is the crystallizer jacket temperature, T_0 is the initial crystallizer temperature, ΔH_c is the enthalpy of crystallization, ρ is the density of the continuous phase, C_p is the specific heat capacity, A_c and U_c are the area and the overall heat transfer coefficients between the crystallizer wall and the jacket stream T_j, respectively, and the values for the process parameters are presented in Table 2.

Table 2. Parameters for the Batch Crystallizer Model

ρ_c	1400	mg/cm^3
ΔH_c	−4.5	kJ/kg
$\rho(t)$	1000 + $C(t)$	mg/cm^3
C_p	4.13	kJ/K·kg
V_{batch}	1	L
A_c	0.25	m^2
U_c	1800	kJ/m^2·h·K
C_0	42	mg/cm^3
T_0	17	°C

Population Balance Equation. The population balance equation (PBE) that describes the evolution of the crystal volume distribution for the batch crystallization process with crystal nucleation and growth can be presented as follows:

$$\frac{\partial n(V,t)}{\partial t} + \frac{\partial (G_{vol}(V,\sigma)n(V,t))}{\partial V} = B\delta(V) \tag{6}$$

where B is the nucleation rate, $\delta(\cdot)$ is the dirac delta function, and $G_{vol}(V,\sigma)$ is the volumetric crystal growth rate, which will be precisely formulated in the following section. Additionally, we assume that, at time t = 0 s, there are no crystals inside the batch crystallizer. This PBE will be used for the design of a moment model in the following section.

Moment Models. In order to deal with the complexity in directly utilizing eq 6 for the numerical computation of a crystal volume distribution in real time, the method of moments is applied to eq 6, and moment models that describe the dominant dynamics, including the evolution of the number of crystals (i.e., zeroth moment M_0) and the total volume (i.e., first moment M_1) of crystals in the batch process, are obtained. This moment model can then be used for the design of an MPC. The jth moment is defined as $M_j(t) = \int_0^\infty V^j n(V,t)\, dV$. For the zeroth moment,

$$\frac{dM_0}{dt} = B \tag{7}$$

and for $j \geq 1$, the jth moment equation has the following form:

$$\frac{dM_j}{dt} = jG_{vol}M_{j-1} \tag{8}$$

Prediction of Crystal Shape. Based on the assumption that the geometry of the HEW lysozyme crystals is a rectangular prism,[25] the volumetric crystal growth rate is formulated as follows:

$$G_{vol} = 2G_{110}\langle h_{110}\rangle\langle h_{101}\rangle + G_{101}\langle h_{110}\rangle^2 \tag{9}$$

where $\langle h_{110}\rangle$ and $\langle h_{101}\rangle$ are the average crystal heights in the direction of (110) and (101) faces, which can be computed as

$$\frac{d\langle h_{110}\rangle}{dt} = G_{110} - \frac{BV_{batch}\langle h_{110}\rangle}{M_0}$$
$$\frac{d\langle h_{101}\rangle}{dt} = G_{101} - \frac{BV_{batch}\langle h_{101}\rangle}{M_0} \tag{10}$$

where G_{110} and G_{101} are the crystal growth rates in the direction of (110) and (101) faces, respectively. The following expressions are calibrated with the experimental data[26] for 2.1 $\leq \sigma \leq$ 4.1 and are used in the MPC in order to predict the dynamic behavior of the crystal growth rates on each face:

$$G_{110} = 0.1843\sigma^3 - 1.1699\sigma^2 + 2.8885\sigma - 2.5616$$
$$G_{101} = 0.1893\sigma^3 - 1.2264\sigma^2 + 2.9887\sigma - 2.5348 \tag{11}$$

R2R-BASED MODEL PREDICTIVE CONTROL

Model Predictive Control Formulation. In this section, we initially propose a model predictive controller (also called MPC) that will be used to compute a set of optimal jacket temperatures, which will lead to the production of crystals with a desired shape distribution at the end of the batch. The moment models (cf. eqs 7 and 8) are derived from a population balance model and used along with the mass and energy balance equations to describe the dominant dynamic behavior of the batch crystallization process. The growth rate equations are computed from open-loop kMC simulations. The design parameters for the proposed R2R-based MPC are chosen so that the proposed R2R-based MPC computes an optimal temperature profile for the production of crystals with a desired shape distribution. An objective function (cf. eq 12a) is defined by the sum of squared errors of the average crystal shape from a desired set-point value throughout the prediction horizon. The jacket temperature is used as a manipulated input, and constraints on the range of temperatures in the crystallizer and the rate of change of the jacket temperature are imposed (cf. eq 12b). The average crystal height on each face is updated according to eq 12g, and the volumetric growth rate is computed through eq 12h. The resulting MPC formulation is given by the following optimization problem:

dx.doi.org/10.1021/ie502377a | Ind. Eng. Chem. Res. 2015, 54, 4293−4302

$$\min_{T_{j,1},\ldots,T_{j,i},\ldots,T_{j,p}} \quad \sum_{i=1}^{p} (\langle\alpha(t_i)\rangle - \alpha_{set})^2 \tag{12a}$$

$$\text{s.t.} \quad 4\ ^\circ\text{C} \le T \le 25\ ^\circ\text{C}, \quad \left|\frac{T_{j,i+1} - T_{j,i}}{\Delta}\right| \le 2\ ^\circ\text{C/min} \tag{12b}$$

$$G_{110} = 0.1843\sigma^3 - 1.1699\sigma^2 + 2.8885\sigma - 2.5616 \tag{12c}$$

$$G_{101} = 0.1893\sigma^3 - 1.2264\sigma^2 + 2.9887\sigma - 2.5348 \tag{12d}$$

$$s = 0.0109T^2 - 0.1146T + 1.1773 \tag{12e}$$

$$\frac{dM_0}{dt} = B, \quad \frac{dM_1}{dt} = G_{vol}M_0 \tag{12f}$$

$$\frac{d\langle h_k\rangle}{dt} = G_k - \frac{BV_{batch}\langle h_k\rangle}{M_0}, \quad k \in \{110, 101\} \tag{12g}$$

$$G_{vol} = 2G_{110}\langle h_{101}\rangle\langle h_{110}\rangle + G_{101}\langle h_{110}\rangle^2 \tag{12h}$$

$$\frac{dC}{dt} = -\frac{\rho_c}{V_{batch}}\frac{dM_1}{dt} \tag{12i}$$

$$\frac{dT}{dt} = -\frac{\rho_c\Delta H_c}{\rho C_p V_{batch}}\frac{dM_1}{dt} - \frac{U_c A_c}{\rho C_p V_{batch}}(T - T_{j,i}) \tag{12j}$$

$$\langle\alpha(t)\rangle \approx \frac{\langle h_{110}(t)\rangle}{\langle h_{101}(t)\rangle}, \quad \langle V(t)\rangle = \frac{M_1(t)}{M_0(t)}, \quad \sigma = \ln(C/s) \tag{12k}$$

where $p = 10$ is the number of prediction steps, $\Delta = 40$ s is the sampling time, $t_i = t + i\Delta$ is the time of the ith prediction step, and $T_{j,i}$ is the jacket temperature of the ith prediction step. At every sampling time, a set of optimal jacket temperatures, ($T_{j,1}$, $T_{j,2}$, ..., $T_{j,p}$), is computed by solving eq 12 with new measurements (C and T) received from the crystallizer (i.e., kMC simulation), and the first value, $T_{j,1}$, is applied to the crystallizer until the next sampling time.

Batch-to-Batch Parameter Estimation. The uncertainty associated with the solubility is modeled by multiplying correction factors, γ_{s1}, γ_{s2}, and γ_{s3}, to the coefficients of the second-order polynomial equation (cf. eq 13c). Similarly, the uncertainty in the crystal growth rate, which is important because the growth mechanisms depend on the supersaturation level, is reflected by multiplying γ_{110}, γ_{101} to the nominal growth rate expressions (cf. eq 13d). Specifically, the spiral growth will dominate at low supersaturation while 2-D nucleation is a prevailing mechanism at high supersaturation.[27]

In this work, an MOP is proposed in order to estimate the system parameters using the post-batch measurements. The correction factors, $\underline{\Gamma} = [\gamma_{110}\ \gamma_{101}\ \gamma_{s1}\ \gamma_{s2}\ \gamma_{s3}]$, are chosen as the decision variables in the MOP. An objective function consists of the sum of squared errors of the predicted average values of the crystal size and shape distributions at the end of the batch process from the measurements. Additionally, the real-time measurements (C, T) throughout the batch are imposed as constraints in eq 13f to make sure the predicted values are close to the measured ones where ε_C and ε_T are tolerances, and another constraint is imposed in eq 13g for the viability of the computed decision variables. The post-batch measurements ($\langle\alpha\rangle$, $\langle V\rangle$, and M_0) are used in eqs 13a and 13e. Note that $\hat{X}_k$ is a predicted variable X for the kth batch run and X_k represents a measured variable X after the kth batch run. The resulting optimization problem is as follows:

$$\min_{\underline{\Gamma}} \quad w_1(\widehat{\langle\alpha(t_f)\rangle}_k - \langle\alpha(t_f)\rangle_k)^2 + w_2(\widehat{\langle V(t_f)\rangle}_k - \langle V(t_f)\rangle_k)^2 \tag{13a}$$

$$\text{s.t.} \quad \text{eqs (12c)}-\text{(12k)} \tag{13b}$$

$$\hat{s} = 0.0109\gamma_{s1}T^2 - 0.1146\gamma_{s2}T + 1.1773\gamma_{s3} \tag{13c}$$

$$\hat{G}_{110} = \gamma_{110}G_{110}, \quad \hat{G}_{101} = \gamma_{101}G_{101} \tag{13d}$$

$$\hat{M}_0(t_f) = M_0(t_f) \tag{13e}$$

$$|\hat{C}_k(t) - C(t)| \le \varepsilon_C, \quad |\hat{T}_k(t) - T(t)| \le \varepsilon_T \tag{13f}$$

$$\underline{l}_\Gamma \le \underline{\Gamma}^T \le \underline{u}_\Gamma \tag{13g}$$

Remark 1. *It is important to note that, although linearly appearing parametric uncertainties are considered in the present work, certain classes of nonlinearly appearing parametric uncertainties can be expressed as linear with suitable definitions of the nonlinear terms in which the uncertain parameters appear with linear terms; thus, they can be readily addressed within the proposed framework. In general, the handling of nonlinearly appearing parametric uncertainties may lead to the need to solve constrained, nonlinear optimization problems—a task that can be handled with the current optimization solvers, particularly given the off-line nature of the parameter estimation calculations.*

Remark 2. *Typically, the post-batch measurements are conducted off-line; thus, the measurement noise is relatively smaller than that of real-time online measurements. Therefore, it is assumed that the accuracy of the post-batch measurements used in this work is acceptable.*

Run-to-Run Control Implementation Algorithm. In general, there are many different ways that an R2R controller can be formulated, and the control performance is mainly determined by the design of the observer, where a simple model may be an average of consecutive errors or may be as complicated as a Kalman filter.

For the batch crystallization process with changes in the process parameters, the PAC scheme can be used. However, if there are too many process parameters to estimate, a large number of measurements may be required for sufficient accuracy. Furthermore, by the time we have sufficient data to estimate the process model parameters, they might have drifted significantly.[15] In this situation, using PAC may further increase the offset. To deal with this issue, the following EWMA control scheme is proposed along with eq 13 for the computation of inputs in the MPC as follows:

$$\widehat{\langle\alpha(t_f)\rangle}_k = f(\hat{\underline{\Gamma}}_k) + \hat{e}_k \tag{14}$$

where $\widehat{\langle\alpha(t_f)\rangle}_k$ is the predicted average crystal shape at the end of the kth batch, $f(\hat{\underline{\Gamma}}_k)$ is a nonlinear equation that consists of eqs 12c−12k and depends on the system parameters $\hat{\underline{\Gamma}}_k$, and $\hat{e}_k$ is the estimated model prediction error. A schematic representation of the proposed R2R-based MPC structure is illustrated in Figure 2.

1. During the kth batch run, the real-time measurements of C_k and T_k are available from the batch crystallization process, and $\hat{\underline{\Gamma}}_k$ is used in the MPC to compute a set of optimal jacket temperatures T_j that will drive the temperature T in the crystallizer to a desired value.

dx.doi.org/10.1021/ie502377a | Ind. Eng. Chem. Res. 2015, 54, 4293−4302

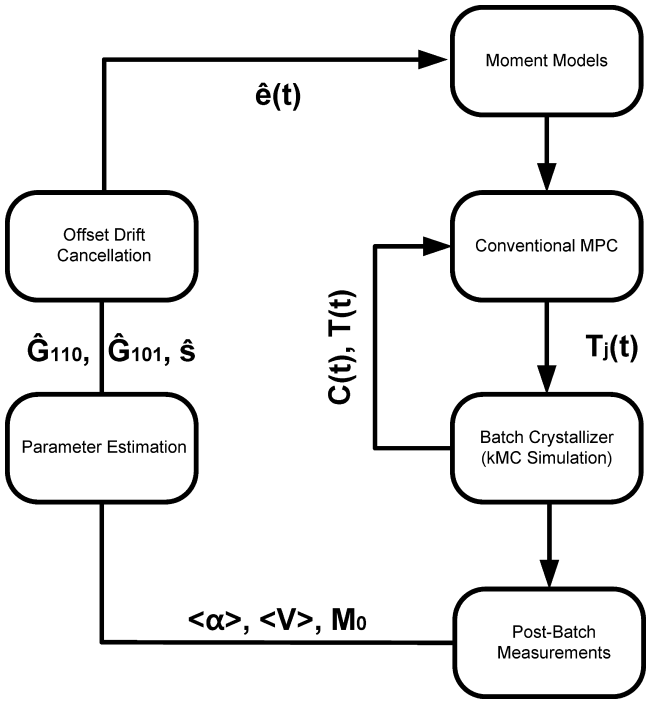

Figure 2. Closed-loop system under R2R-based MPC scheme.

2. At the end of the kth batch process, the post-batch measurements of product qualities such as average crystal size, shape, and number of crystals are measured and used to re-compute $\hat{\underline{\Gamma}}_{k+1}$ by solving eq 13.
3. The model prediction error is updated recursively through a weighted average, $\hat{e}_{k+1} = (1 - \lambda)\hat{e}_k + \lambda(\langle\alpha(t_f)\rangle_k - f(\hat{\underline{\Gamma}}_k))$, where $0 < \lambda \leq 1$ is the learning factor.
4. During the k+1th batch run, the predicted average crystal shape $\widehat{\langle\alpha(t_f)\rangle}_{k+1}$ is computed through eq 14 and used in the MPC to compute a set of optimal T_j values.
5. Increase k by 1 and repeat steps 1−5.

Remark 3. *In general, the learning factor can be understood as a process gain in the conventional P-controller in that a high λ would guarantee fast convergence while a low λ is preferred for stability of the controlled output. Therefore, the trade-off between fast convergence and stability has to be evaluated by a trial-and-error procedure. Note that the nominal system parameters are used a priori for $\hat{\underline{\Gamma}}_0$, and it is assumed that there is no parametric model mismatch in the beginning (i.e., $\hat{e}_0 = 0$).*

Remark 4. *Both ideas of an offset drift cancellation (ODC) scheme and an parameter adaptive control (PAC) schemes are used in the proposed R2R-based MPC along with a conventional MPC to reduce the offset while simultaneously achieving fast convergence. Therefore, the proposed R2R-based MPC is able to deal with the parametric mismatch (i.e., inherent variation) of crystal nucleation and growth rates as well as the process drift by adapting the process model parameters through the parameter estimation algorithm described above (cf. eq 13), which cannot be done by a conventional MPC with a nominal process model (cf. eq 12). Because of the predictive ability of an MPC, the proposed R2R-based MPC is also able to predict the evolution of crystal shape with good accuracy during the process when the measurements of the product qualities are not available, which will lead to an improvement in the control performance achieving the production of crystals with a desired shape distribution.*

SIMULATION RESULTS

There are many factors, including the pH and the concentration of added electrolyte (e.g., NaCl), that affect the solubility of a system. Because of a change in the solubility, the crystallization process parameters to be estimated can be perturbed from a nominal operation regime, which may lead to a poor control performance unless appropriate adjustments are made to the nominal process model used in the MPC. In order to evaluate the control performance of the proposed R2R-based MPC in the presence of variation in the solubility, the pH value used in the kMC simulation (representing the batch crystallization process) is perturbed to 4.5 from the nominal value 4.4, while the NaCl concentration remains constant at 4%. This causes roughly 50% drop in the solubility level. Furthermore, a process drift with a rate at which it takes 50 batch runs for solubility to completely drift 5% from its nominal value is applied to the batch crystallization process, which is consistent with the one defined in ref 10 for a slowly drifting process.

Typically, an ODC controller is used to deal with the process drift, and it is robust with respect to the process drift at the expense of using less aggressive control actions. On the other hand, a parameter adaptive controller is preferred in order to achieve a fast convergence if a correct process model is assumed, but the control performance can be degraded if there are many process model parameters to estimate compared to the number of measurements available. Therefore, it is important to choose which controller type to use, depending on the goal we want to achieve.

In this work, the ideas of both the ODC and parameter adaptive controllers are integrated with a conventional MPC such that the proposed R2R-based MPC directly adapts the model parameters and at the same time handles the remaining offset through an EWMA-type control scheme. In Figure 3, it is presented that the proposed R2R-based MPC with $\lambda = 0.3$ is able to achieve the production of crystals with a desired crystal shape distribution after three iterations (i.e., fast convergence), while the control performance of a conventional MPC with nominal system parameters (cf. eq 12) becomes progressively

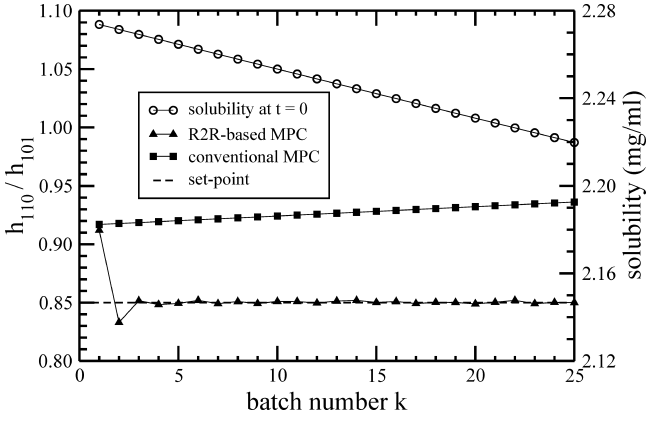

Figure 3. Evolution of the average crystal shape at t = 20 000 s obtained from the kMC simulations from batch to batch under the conventional MPC and R2R-based MPC with the desired set-point $\langle\alpha_{set}\rangle$ = 0.85. Additionally, the drift of the solubility profile from the nominal model is plotted.

dx.doi.org/10.1021/ie502377a | Ind. Eng. Chem. Res. 2015, 54, 4293−4302

worse as runs are repeated, owing to process drift and variability.

For comparison purposes, the proposed R2R-based MPC scheme is compared with an EWMA-type CSC strategy, where its desired set-point (i.e., supersaturation) for the kth batch run is updated as is described below.

1. The desired supersaturation level $\sigma_{\text{set},k}$, which will be applied to the kth batch run, can be computed as follows:

$$s_{\text{set},k} = s_{\text{set},k-1} + d_k$$

where the correction factor d_k has the form

$$d_k = d_{k-1} + \lambda(\langle\alpha(t_f)\rangle_{k-1} - \alpha_{\text{set}})$$

2. At the end of the kth batch run, the average crystal shape $\langle\alpha(t_f)\rangle_k$ is measured.
3. Increase k by 1 and repeat steps 1−3.

As is shown in Figure 4, although both control schemes are able to produce crystals with a desired shape distribution after

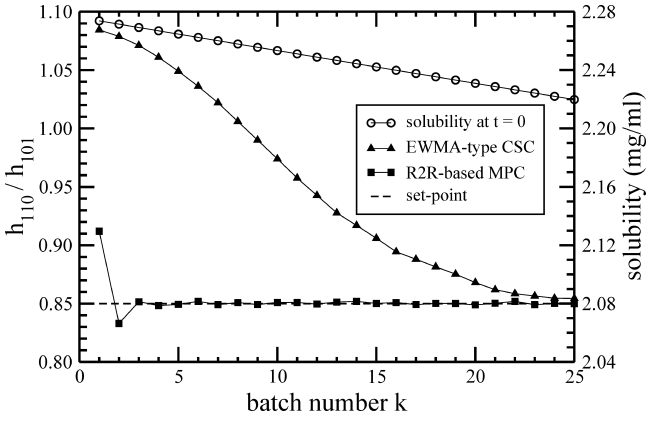

Figure 4. Evolution of the average crystal shapes at t = 20 000 s obtained from the kMC simulations from batch to batch under the EWMA-type CSC and R2R-based MPC. The desired set-point is $\langle\alpha_{\text{set}}\rangle$ = 0.85. Additionally, the drifted of the solubility profile from the nominal model is plotted.

multiple runs, the convergence of the EWMA-type CSC is significantly slower than that of the proposed R2R-based MPC (24 runs vs 3 runs to achieve the same performance). Furthermore, the crystal shape distribution obtained by the proposed R2R-based MPC in Figure 5 is closer to the desired set-point value, $\langle\alpha_{\text{set}}\rangle$ = 0.85, than that of the EWMA-type CSC. The superiority in the control performance of the proposed R2R-based MPC over the EWMA-type CSC and conventional MPC without R2R model adaptation is because of the parameter estimation step implemented in the proposed R2R-based MPC that effectively estimates the process model parameters by solving eq 13 with the post-batch measurements received from the previous run. As a result, the predicted solubility value approaches to the actual solubility value as is shown in Figure 6 with an about 2% offset between the two profiles. The remaining offset induced by the process drift introduced to the current batch crystallization process is properly handled by an EWMA scheme (i.e., steps 3 and 4 in the proposed R2R-based MPC); thus, in Figure 7, the solubility at the end of each batch is successfully regulated to a constant value.

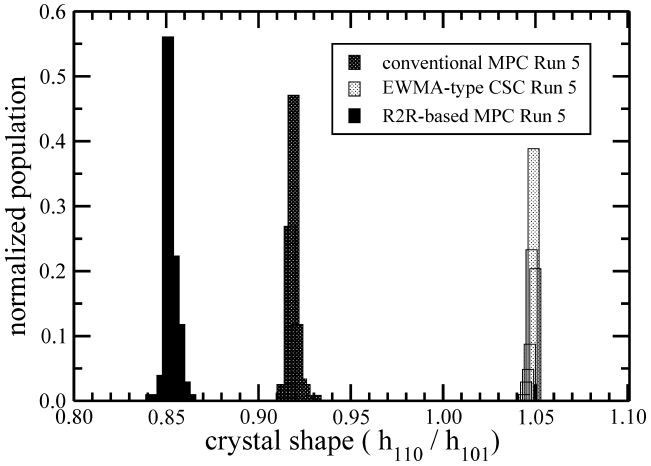

Figure 5. Normalized crystal shape distributions at t = 20 000 s obtained from the kMC simulations under the conventional MPC, EWMA-type CSC, and R2R-based MPC. The desired set-point is $\langle\alpha_{\text{set}}\rangle$ = 0.85.

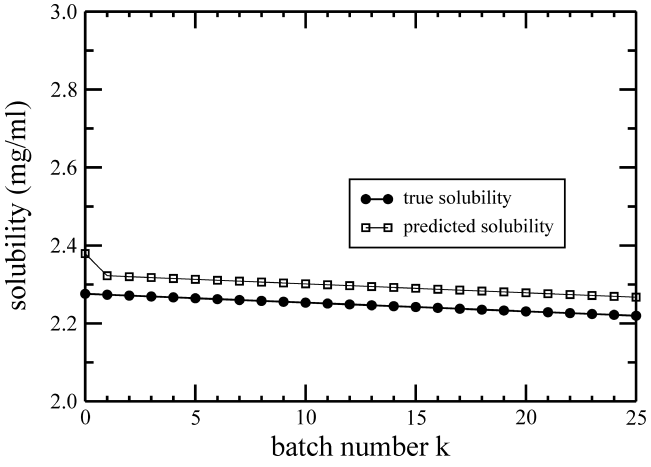

Figure 6. Evolution of the predicted and true solubilities in the beginning of batch runs from batch to batch under the R2R-based MPC. The discrepancy between the two profiles is about 2%.

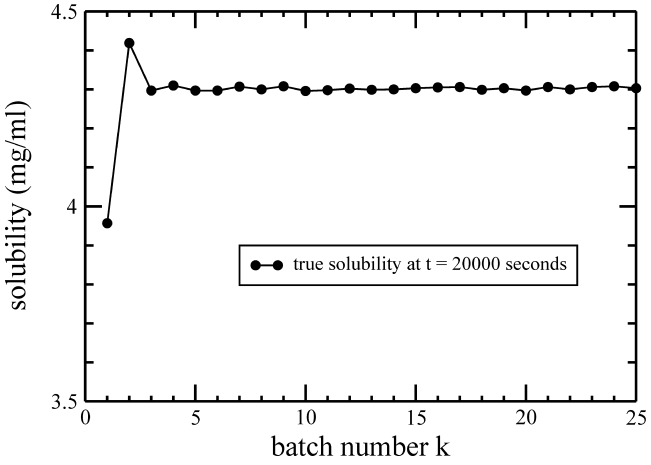

Figure 7. Evolution of the solubility at the end of batch runs from batch to batch under the R2R-based MPC.

Furthermore, a comparison of a conventional MPC with an ODC and APC scheme is shown in Figure 8. A conventional MPC with a PAC scheme converges fast (after three iterations)

dx.doi.org/10.1021/ie502377a | Ind. Eng. Chem. Res. 2015, 54, 4293−4302

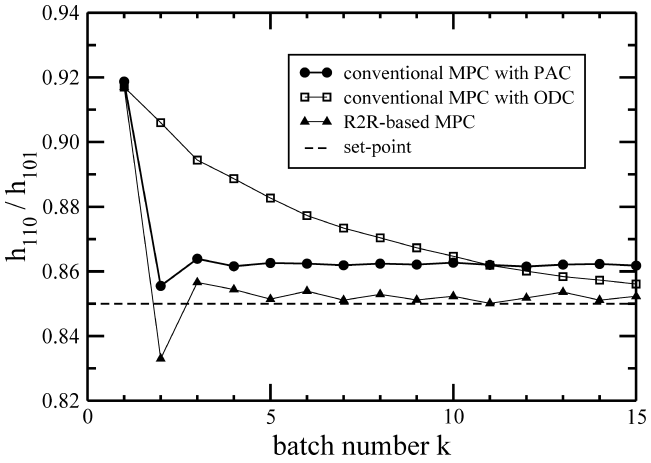

Figure 8. Evolution of the average crystal shape at t = 20 000 s obtained from the kMC simulations from batch to batch under the conventional MPC with ODC and PAC, respectively, and the R2R-based MPC. The desired set-point is $\langle\alpha_{set}\rangle$ = 0.85.

but with a persistent offset, while a conventional MPC with an ODC converges slowly but eventually will produce crystals with a desired shape. Therefore, both the ODC and APC schemes in the proposed R2R-based MPC are needed, along with a conventional MPC, to reduce the offset while simultaneously achieving fast convergence.

In Figures 9 and 10, the jacket temperature profiles for the process under EWMA-type CSC and R2R-based MPC at

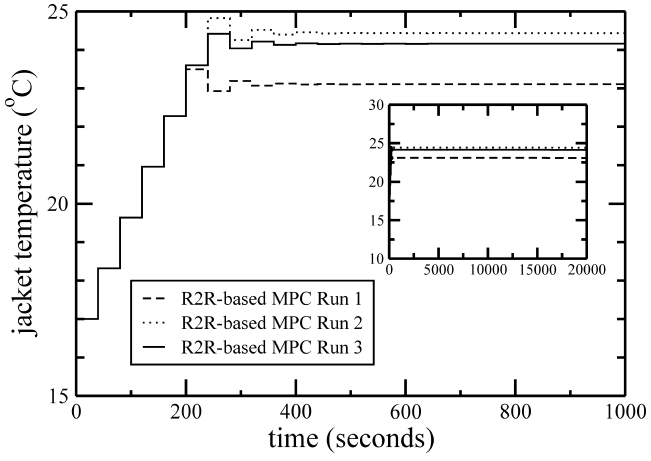

Figure 9. Evolution of the jacket temperature (T_w) computed by solving the R2R-based MPC with respect to time for t < 1000 s when the desired set-point is $\langle\alpha_{set}\rangle$ = 0.85. The inset shows the T_w profile from t = 0 to t = 20 000 s.

different batch runs are presented. Note that the jacket temperature profiles reach the optimal condition relatively fast in the beginning and remain constant throughout the process. Moreover, the temperature profile over the entire batch run is added as an inset to each figure.

In addition to the constant process drift rate (i.e., 0.1% drop per batch) introduced to the simulations discussed above, a random process drift with an exponential distribution and a decaying process drift are also introduced to closed-loop simulations in order to evaluate the robustness of the proposed R2R-based MPC with respect to different types of process drift. As is presented in Figure 11, the type 1 process drift is a

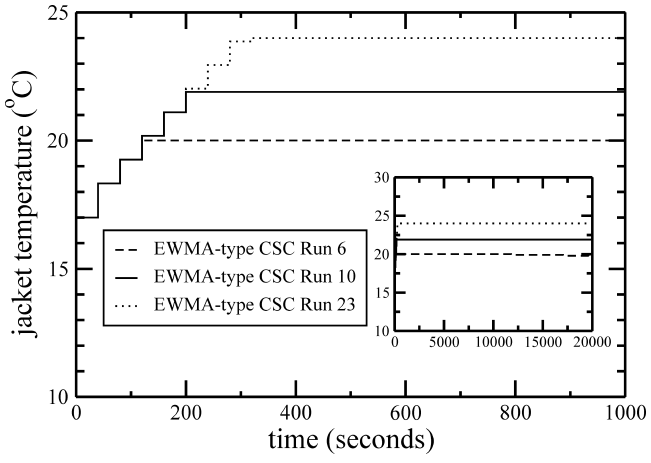

Figure 10. Evolution of the jacket temperature (T_w) computed by solving EWMA-type CSC with respect to time for t < 1000 s when the desired set-point is $\langle\alpha_{set}\rangle$ = 0.85. The inset shows the T_w profile from t = 0 to t = 20 000 s.

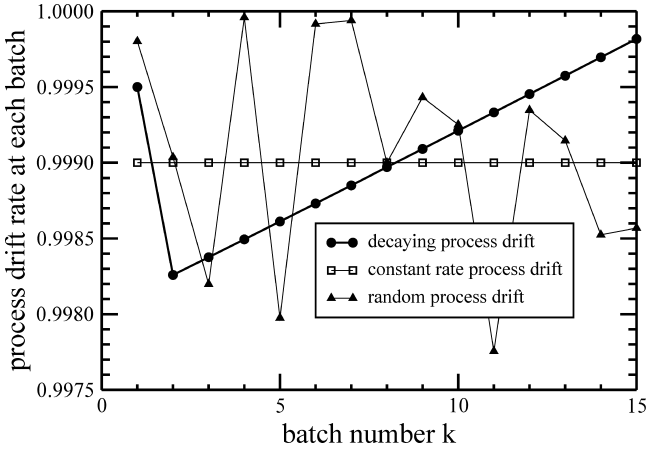

Figure 11. Evolution of the process drift rate from batch to batch. The rate of the process drift type 1 follows a decaying curve; type 2 follows a constant; and type 3 follows an exponential distribution.

decaying process drift, where the process drift rate slows down as runs are repeated, which is the most prevailing type of drift in the industry.[11] Type 2 is a process drift with a constant rate, and type 3 is a process drift where its rate (i.e., variation from batch to batch) follows an exponential distribution. Note that the means of the type 2 and type 3 process drifts are identical, at 0.1% drop per batch, and the y-axis implies how much the system has drifted from a nominal system after each batch run. Thus, the value 1 in the y-axis indicates that it is a nominal system, and the value becomes lower as the system drifts away from a nominal system. Additionally, the cumulative process drifts are shown in Figure 12, where the decaying characteristic of the type 1 process drift is more evident. Similar to Figure 7, the parametric mismatches in the solubility induced by different types of the process drifts are successfully handled. It is apparent from Figure 13 that the control performances of the proposed R2R-based MPC in response to the type 1 and type 3 process drifts are worse than that of the type 2 process drift. In particular, the control performance for the system with the type 3 process drift is even worse than that of the type 1 process drift because the type 3 process drift changes more drastically, which is difficult to compensate for quickly through the

dx.doi.org/10.1021/ie502377a | Ind. Eng. Chem. Res. 2015, 54, 4293−4302

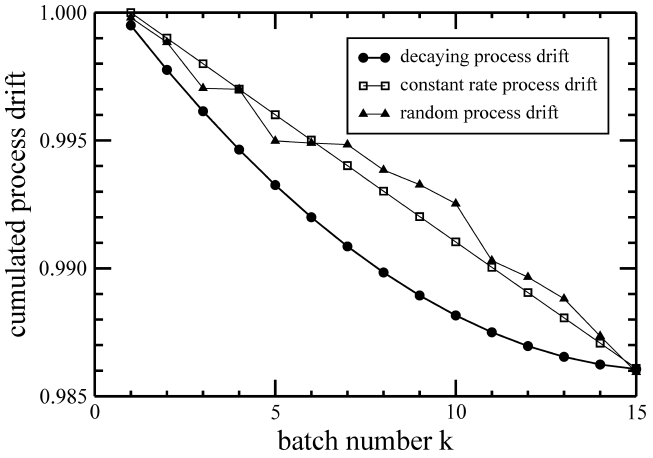

Figure 12. Evolution of the cumulative process drift from batch to batch that indicates how much the real system has been drifted from an initial nominal system. The rate of the process drift type 1 follows a decaying curve; type 2 follows a constant; and type 3 follows an exponential distribution.

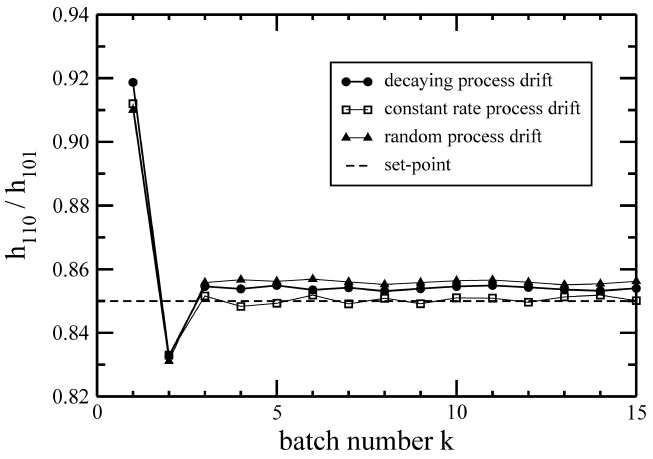

Figure 13. Evolution of the average crystal shape obtained from the kMC simulations from batch to batch under the R2R-based MPC with three different process drift types described in Figure 12. The rate of the process drift type 1 follows a decaying curve; type 2 follows a constant; and type 3 follows an exponential distribution.

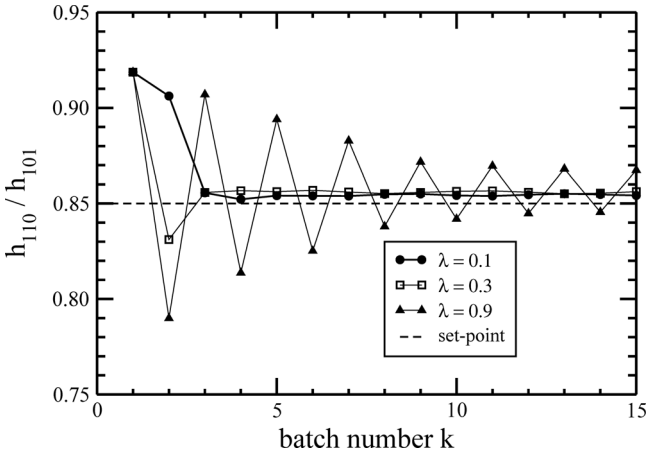

Figure 14. Evolution of the average crystal shape obtained from the kMC simulations from batch to batch under the R2R-based MPC for λ = 0.1, 0.3, and 0.9, with the type 3 process drift described in Figure 12.

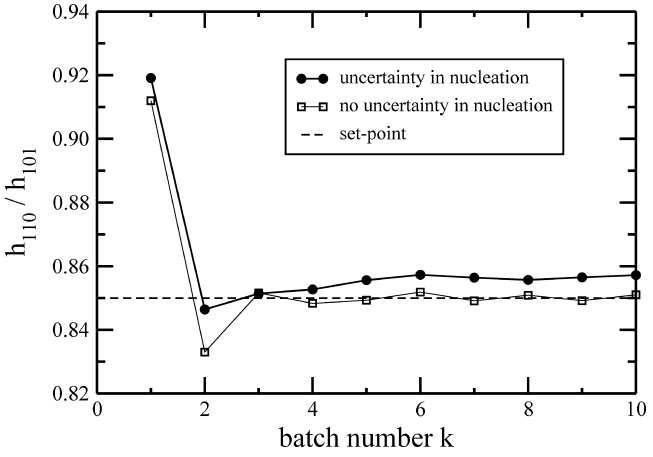

Figure 15. Evolution of the average crystal shape obtained from the kMC simulations from batch to batch under the R2R-based MPC for two cases when there is an unmodeled uncertainty in the nucleation rate vs no uncertainty in the nucleation rate. The desired set-point is $\langle \alpha_{set} \rangle$ = 0.85.

proposed R2R-based MPC. This offset might become more significant if the process drift changes more frequently with a greater magnitude. As presented in Figure 14, for a high λ value, the proposed R2R-based MPC becomes vulnerable to the rapidly changing process drift introduced to the system, while this effect is relatively suppressed by using small λ values in the proposed R2R-based MPC. One potential solution to this problem is to adapt the learning factor λ after each batch to properly deal with the varying process drift rate.

Finally, for the purpose of testing the control performance with respect to unmodeled uncertainty in the nucleation rate from a controller point of view, the nucleation rate in the kMC simulation is deliberately reduced by 10% by multiplying eq 1 by 0.9. Since this uncertainty is not modeled in the controller process model, the other parameters, $\underline{\Gamma} = [\gamma_{110}\ \gamma_{101}\ \gamma_{s1}\ \gamma_{s2}\ \gamma_{s3}]$, must be adjusted to compensate for the unmodeled uncertainty in the nucleation rate. Furthermore, the equality constraint (cf. eq 13e) enforces the proposed R2R-based MPC with an estimated parameter to produce the same number of crystals as the previous batch run. As a result, it is shown in Figure 15 that the controller model parameters are appropriately adjusted, and thus the effect of the unmodeled uncertainty on the control performance is properly mitigated, producing crystals with a shape that is close to the desired set-point. However, the closed-loop performance under such an unmodeled uncertainty is slightly degraded, with an offset from a desired set-point. Such minor degradation is expected due to the nonlinear nature of the unmodeled uncertainty in the nucleation rate while the ODC scheme used in the proposed R2R-based MPC is linear. To deal with this problem, a nonlinear ODC scheme could be adopted in order to improve the robustness of the proposed R2R-based MPC with respect to unmodeled uncertainties.

In this work, the closed-loop simulation results show that the average crystal shape distribution is already driven close to a desired value after three batch runs under the proposed R2R-based MPC scheme; hence, varying the learning factor does not notably influence the control performance, as is shown in Figure 16. Therefore, the proposed R2R-based MPC is able to leverage smaller λ values (e.g., λ = 0.1) to reduce the effect of the measurement noise without significantly sacrificing the convergence speed.

dx.doi.org/10.1021/ie502377a | Ind. Eng. Chem. Res. 2015, 54, 4293−4302

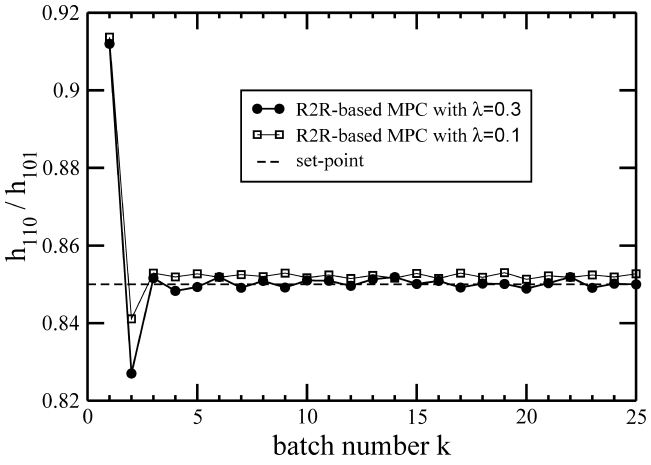

Figure 16. Evolution of the average crystal shape obtained from the kMC simulations from batch to batch under the R2R-based MPC with $\lambda = 0.1$ and $\lambda = 0.3$. The desired set-point is $\langle \alpha_{set} \rangle = 0.85$.

Remark 5. *If the measurement noise is sufficiently high, an R2R controller may fail because the past measurements are not autocorrelated with the future runs.*[28,29] *The best practice to deal with the measurement noise is to use a small learning factor λ in an EWMA design at the cost of slower convergence. Additionally, a low-pass filter may be used to reduce the effects of noise of the measurements (both real-time and postbatch) to the operation of the batch crystallization process.*

CONCLUSIONS

In this work, we considered the design of a novel R2R-based MPC for a batch crystallization process with significant process drift and inherent variation in solubility and crystal growth rates. In order to achieve the production of crystals with desired crystal shape distribution, a conventional MPC with nominal process model parameters (cf. eq 12) was initially applied to the process. However, due to the process drift, the mismatch between the controller model and the process dynamic behavior became severe as batch runs were repeated. To deal with this problem, an R2R-based MPC was proposed in which, after each batch was over, the post-batch measurements, including average crystal shape and size and the number of crystals, were used to estimate off-line the drift of the process model parameters from nominal values via a multivariable optimization problem. Along with the adapted model parameters, the EWMA scheme was used to deal with the remaining offset in the model and thereby to compute via MPC a set of optimal jacket temperatures in real time that drives the process to a desired condition. Furthermore, the crystal growth in the batch crystallization process was modeled through kMC simulations, and this model was then used to demonstrate the ability of the proposed control scheme to suppress the inherent variation and process drift in solubility and crystal growth rates. Through the proposed approach, the production of crystals with a desired shape distribution was successfully achieved after three batch runs through the use of R2R-based MPC, while it took 24 batch runs to achieve this for the system with the EWMA-type CSC strategy.

AUTHOR INFORMATION

Corresponding Authors

*E-mail: dong.ni@ia.ac.cn.

*E-mail: pdc@seas.ucla.edu.

Notes

The authors declare no competing financial interest.

ACKNOWLEDGMENTS

The authors gratefully acknowledge financial support from the Extreme Science and Engineering Discovery Environment (TG-CCR120003), the National Science Foundation (CBET-0967291), and the NSF Graduate Research Fellowship (DGE-0707424, to M.N.).

REFERENCES

(1) Yang, G.; Kubota, N.; Sha, Z.; Louhi-Kultanen, M.; Wang, J. Crystal shape control by manipulating supersaturation in batch cooling crystallization. *Cryst. Growth Des.* **2006**, *6*, 2799−2803.

(2) Shi, D.; El-Farra, N. H.; Li, M.; Mhaskar, P.; Christofides, P. D. Predictive control of particle size distribution in particulate processes. *Chem. Eng. Sci.* **2006**, *61*, 268−281.

(3) Nagy, Z. Model based robust control approach for batch crystallization product design. *Comput. Chem. Eng.* **2009**, *33*, 1685−1691.

(4) Nayhouse, M.; Kwon, J. S.; Christofides, P. D.; Orkoulas, G. Crystal Shape Modeling and Control in Protein Crystal Growth. *Chem. Eng. Sci.* **2013**, *87*, 216−223.

(5) Kwon, J. S.; Nayhouse, M.; Christofides, P. D.; Orkoulas, G. Modeling and control of crystal shape in continuous protein crystallization. *Chem. Eng. Sci.* **2014**, *107*, 47−57.

(6) Rohani, S.; Haeri, M.; Wood, H. Modeling and control of a continuous crystallization process, Part 2: Model predictive control. *Comput. Chem. Eng.* **1999**, *23*, 279−286.

(7) Moldovanyi, N.; Lakatos, B.; Szeifert, F. Model predictive control of MSMPR crystallizers. *J. Cryst. Growth* **2005**, *275*, e1349−e1354.

(8) Nadarajah, S.; Lee, J. Repetitive model predictive control applied to a simulated moving bed chromatography system. *Comput. Chem. Eng.* **2000**, *24*, 1127−1133.

(9) Sachs, E.; Guo, R.; Ha, A. On-line process optimization and control using the sequential design of experiments. *Symp. VLSI Technol., 1990, Dig. Tech. Pap.* **1990**, 99−100.

(10) Sachs, E.; Hu, A.; Ingolfsson, A. Run by run process control: combining SPC and feedback control. *IEEE Trans. Semicond. Manuf.* **1995**, *8*, 26−43.

(11) Moyne, J.; Castillo, E. D.; Hurwitz, A. M. *Run-to-run control in semiconductor manufacturing*; CRC Press: Boca Raton, FL, 2001.

(12) Campbell, W.; Firth, S.; Toprac, A.; Edgar, T. A comparison of Run-to-Run control algorithms. *Proc. Am. Control Conf.* **2002**, *6*, 2150−2155.

(13) Wang, Y.; Gao, F.; Doyle, F. Survey on iterative learning control, repetitive control, and run-to-run control. *J. Process Control* **2009**, *19*, 1589−1600.

(14) Palmer, E.; Ren, W.; Spanos, C.; Poolla, K. Control of photoresist properties: a kalman filter based approach. *IEEE Trans. Semicond. Manuf.* **1996**, *9*, 208−214.

(15) Musacchio, J.; Rangan, S.; Spanos, C.; Poolla, K. On the utility of run to run control in semiconductor manufacturing. *Semicond. Manuf. Conf. Proc.* **1997**, D9−D12.

(16) Lee, J.; Nadarajah, S.; Lee, K. A model-based predictive control approach to repetitive control of continuous processes with periodic operations. *J. Process Control* **2001**, *11*, 195−207.

(17) Hermanto, M.; Braatz, R.; Chiu, M.-S. A run-to-run control strategy for polymorphic transformation in pharmaceutical crystallization. *Proc. IEEE Int. Conf. Control Appl.* **2006**, 2121−2126.

(18) Forgione, M.; Mesbah, A.; Bombois, X.; Van den Hof, P. Batch-to-batch strategies for cooling crystallization. *Proc. 51st IEEE Conf. Decision Control* **2012**, 6364−6369.

(19) Kwon, J. S.; Nayhouse, M.; Christofides, P. D.; Orkoulas, G. Modeling and control of shape distribution of protein crystal aggregates. *Chem. Eng. Sci.* **2013**, *104*, 484−497.

(20) Smejkal, B.; Helk, B.; Rondeau, J.; Anton, S.; Wilke, A.; Scheyerer, P.; Fries, J.; Hekmat, D.; Weuster-Botz, D. Protein

crystallization in stirred systems-scale-up via the maximum local energy dissipation. *Biotechnol. Bioeng.* **2013**, *110*, 1956−1963.
(21) Galkin, O.; Vekilov, P. G. Nulceation of protein crystals: critical nuclei, phase behavior, and control pathways. *J. Cryst. Growth* **2001**, *232*, 63−76.
(22) Cacioppo, E.; Pusey, M. L. The solubility of the tetragonal form of hen egg white lysozyme from pH 4.0 to 5.4. *J. Cryst. Growth* **1991**, *114*, 286−292.
(23) Durbin, S. D.; Feher, G. Simulation of lysozyme crystal growth by the Monte Carlo method. *J. Cryst. Growth* **1991**, *110*, 41−51.
(24) Ke, S. C.; DeLucas, L. J.; Harrison, J. G. Computer simulation of protein crystal growth using aggregates as the growth unit. *J. Phys. D: Appl. Phys.* **1998**, *31*, 1064−1070.
(25) Kwon, J. S.; Nayhouse, M.; Orkoulas, G.; Christofides, P. D. Enhancing crystal production rate and reducing polydispersity in continuous protein crystallization (in press). *Ind. Eng. Chem. Res.* **2014**, DOI: 10.1021/ie5008163.
(26) Durbin, S. D.; Feher, G. Crystal growth studies of lysozyme as a model for protein crystallization. *J. Cryst. Growth* **1986**, *76*, 583−592.
(27) Burton, W. K.; Cabrera, N.; Frank, F. C. The growth of crystals and the equilibrium structure of their surfaces. *Philos. Trans. R. Soc.* **1951**, *243*, 299−358.
(28) Muth, F. Optimal properties of exponentially weighted forecasts of time series with permanent and transitory components. *J. Am. Stat. Assoc.* **1960**, *55*, 239−250.
(29) Ingolfsson, A.; Sachs, E. Stability and sensitivity of an EWMA controller. *J. Quality Technol.* **1993**, *25*, 271−287.